

Formation of a hard surface layer during drying of a heated porous media

Navneet Kumar, Jaywant H Arakeri, Musuvathi S Bobji

Department of Mechanical Engineering

Indian Institute of Science, Bangalore – 560012, India

We report surface hardening or crust formation, unlike caking, during drying when a confined porous medium was heated from above using IR radiation. These crusts have higher strength than their closest counterparts such as sandcastles and mud-peels which essentially are clusters of partially wet porous medium. Observed higher strength of the crusts is mostly due to surface tension between the solid particles which are connected by liquid bridges (connate water). Qualitative (FTIR) and quantitative (TGA) measurements confirm the presence of trapped water within the crust. Amount of the trapped water was ~1.5% (this is about 10 times higher than in the samples with caking) which was confirmed using SEM images. Further, in the fixed particle sizes case, the crust thickness varied slightly (10-20 particle diameters only for cases with external heating) while with the natural sand whole porous column was crusted; surprisingly, crust was also found with the hydrophobic glass beads. Fluorescein dye visualization technique was used to determine the crust thickness. We give a power law relation between the crust thickness and the incident heat flux for various particle sizes. The strength of the crust decreases drastically with increasing hydrophilic spheres diameter while it increases with higher surface temperature.

Introduction

Evaporation is ubiquitous in nature, from bare water surfaces, soils, and plants, and is useful in many industrial applications. Of major interest is evaporation from soil, a porous medium, due to its complexities such as a vast range of particle sizes, local textural contrasts etc. The formation of soil crusts, as it runs dry, has been argued mainly due to two factors namely (a) biological and (b) physical. The continuous heating and cooling process, so called the freeze-thaw action, along with the rainfall effects have been held responsible for the crusting of the upper layers. Thus along with leaching, rainfall seems equally important in the formation of physical soil crusts. The hardening of soils is thus a common observation in nature whether it is in the form of mud-peels or soil crusts. Mudcracks followed by peeling off of a thin soil layer (mud-peeling) is a common observation when a water source (such as a pond, lake, or a river) runs dry for a long time. Scientists have long puzzled over the formation of these cracks while the phenomenon of mud-peeling has hardly been explored. Numerous experiments successfully imitated cracking in the laboratory [1-8] and in field [9,10] but only a few of them observed the mud-peels [1,6]. These experiments were conducted with river bed sand [1], starch solution [3], coffee water mixture [2], suspension of latex particles [5], cement [9,10], and concretes [7]. Peeling-off (followed by cracking) of colloidal suspensions [11-17] such as wet paints during and after its drying (once it has been applied on a surface) is another commonly observed phenomenon. It has been shown that the cracking mechanism is different for the soft and hard particles. Evaporation leads to compressive capillary forces on the particles [11,18,19] and in case of hard particles, cracking is a pressure release mechanism [9,13]. Mud-peels (Figure S1c), in general, are flakes of thin layer of particles adhered (via traces of water or salt or some other chemical reaction based mechanisms) together providing it some strength compared to the layer just below it. 'Leaching', loss of nutrients in the form of minerals and salts, brings salt to the top and deposit them in a few top (exposed to the ambient) layers of soils making it hard [20-22]. It has been known for quite some time that addition of a small amount of water changes the soil strength significantly [23]. On the other hand fully saturated and fully unsaturated soils have been found not to resist the shear force and hence could be treated as having no strength at all.

Evaporation from a confined porous medium [24,25] has been shown to undergo three different stages; these stages also existed for other porous systems such as texturally layered [26], stack of rods [27], and stack of plates [28]. Recently, with horizontal stack of rods, it was shown [29] that the rods' surface roughness is important in deciding the duration of these stages. In the 1st stage, a porous medium sustains higher evaporation rate (close to that from a bare water surface) which has been shown to be due to the presence of water [25,26,28] near the porous medium top surface. Note that, in these type of processes, the competition is between the gravitational and interfacial forces while the viscous effects have been suggested [24,30,31] to be taken into account either when the evaporation rates are very high or when the particle sizes are large or both. Water on the porous medium top surface is supported by the capillary water films [32-34] which connects water near the top to the deeper regions within the porous medium. Regions which are drained-off of water, by the capillary films, are not fully drained, a small amount of water gets trapped which is commonly known as pendular structures [23]; co-existence of all the three phases. The (tiny) trapped isolated water exerts enough interfacial force on the solid particles to hold them together [35-37] and is believed to be the main reason behind the formation of sandcastles [38-43] (Figure S1a,b). This property of unsaturated soil has been used to create sharp-cornered structures which would be otherwise impossible if the soil is either fully wet or fully dry [39]. Using fluorescein microscopy, it was shown [40-42] that liquid bridges form at some critical water volume percentage (calculated as the volume of water present or added to the total sample volume) before which water resides within the roughness of the solid spheres. This critical value varied between different studies (it was 0.07% in case of glass beads with an average diameter of $375\mu\text{m}$ [41]) largely due to variation in bead sizes and packing fractions. At some instant (0.2% in [41]) these liquid bridges were fully developed. The number of these bridges per bead increased with increasing water volume and eventually saturated at ~ 6.5 at 0.8% water content; these data were reported [40,41] for the case of random close packing where void fraction was $\sim 36\%$. Further addition of water led to decreasing numbers of bridges [42] as the structure now shifts from pendular to a funicular one [23,43]. The measured tensile strength [42] also increased with increasing addition of water and reached a maximum at 0.015% of water after which it remained constant till 15% of water. A value of 15% of water means that $\sim 35\%$ of available space has been occupied by water; in these experiments the reported packing fraction was ~ 0.57 . For a perfectly wetting liquid bridge, the interfacial force (F), see Figure S11, after the critical water content, remains a constant [35,37,43] and is given as:

$$F = 2\pi R\sigma \quad (1)$$

Where, R is the grain (solid sphere) radius and σ is the interfacial surface tension. It so happens that an increase in the liquid volume is adjusted by a corresponding decrease in the radius of curvature.

Previous investigators added liquids (such as water), in controlled amount, to spheres and measured the soil strength (either shear or tensile) with or without vertical agitation. Their analysis was mostly focussed on the angle of repose and, in particular, finding the critical angle after which the system slumps. Investigators have also studied this 'sticky' nature of partially wet sand during drying [1,7,20,24,33] but none have reported results on the impact of either particle size or the surface temperature. The formation and 1D growth of soil crust (near the air interface), during the drying of a colloidal suspensions, has been modelled (a moving boundary problem) recently [44] where a constant evaporation rate was assumed. Peeling-off of the upper crusted layer is initiated by horizontal cracks which propagate parallel to the drying surface. Note that a horizontal crack forms only if vertical (mudcracks)

cracks are available. It was shown [45] that the gradient in the tensile stress at the drying surface forces the crack to curl up and form a mud peel; similar to ‘spalling’ and ‘caking’. The depth of peeling was also modelled [45] considering a constant water evaporation rate at the drying surface. Apart from a few of these studies there are no concrete evidences behind the formation and strength of the crusts in a drying porous medium.

We report laboratory experiments on the formation of crusts (during drying) in porous media consisting mostly of nearly mono-disperse glass beads; similar sized spheres have been used previously [33,40,42,43]. We have defined ‘crusts’ in our experiments as ‘the hard layer formed, at the side exposed to the ambient, during the drying of a porous medium’. Majority of the experiments were conducted, with de-ionized (DI) water, while heating the samples from above using infrared (IR) radiation. We found that a thin upper (exposed to the open boundary) layer of the sample was crusted (neither very flaky nor like a slump) which fragments into pieces (like a cookie) when broken; this has never been reported previously. We attempt to answer a few fundamental questions like (1) when and where do crusts form, (2) why do they form at all, and (3) how do they form? We further investigate the dependence of the crust properties (such as its thickness and strength) on various controlled parameters such as the surface temperature (or the heat flux incident on the porous medium top surface), particles sizes, and wetting characteristics of the porous medium. A few experiments were also carried out with soil (with a range of particle sizes) and other evaporating liquids.

Materials and Methods

Confined and saturated porous mixtures consisting (mostly) of DI water and glass beads were prepared following a specific protocol [25,46]. Three different diameters viz. nearly mono-disperse 0.10-0.16 mm, 0.40-0.50 mm, and 0.70-0.85 mm, of glass beads (GB) were used; the average sizes can be considered as 0.13, 0.45, and 0.78 mm in the same order. These glass beads are solid, non-porous, and hard; they don’t deform due to interfacial forces. In some experiments, the glass beads were cleaned using piranha solution and in one case sieved natural sand (0.30-0.50 mm particle diameter) was also used. Different evaporating liquid were used such as distilled water, millipore (multi-stage distilled) water, and acetone. Experiments were conducted in different containers, depending on the duration of stage 1, for different purposes. The container containing the porous medium was insulated from all the sides except at the top. The medium saturated with water was heated radiatively using a 20cm x 20cm flat ceramic IR heater from the top. The heater was connected to a variac for controlling the IR intensity which was also controlled by varying its distance from the porous medium. Mass loss was monitored using a precision weighing balance (Sartorius GPA5202 with a least count of 0.01g); mass was recorded on a computer every 15 seconds.

The ambient temperature was measured using a T-type thermocouple. A Honeywell humidity sensor (HIH-4000 with an accuracy of 2%) measured the relative humidity (RH) in the ambient away from the heating area. A data logger (Agilent 34972A) was used to log the temperature from the thermocouples and RH sensor. A schematic of the experimental setup is shown in Figure S2. A thermal camera (Fluke Ti400, 320x240 pixels) was used to monitor the porous medium top surface temperature at different times. Small and large scale experiments are referred to those types of porous media whose heights were much lesser and larger than the capillary characteristic length [25], respectively. Experiments were also conducted with hydrophobic glass beads; a standard technique [47] was used to make glass beads hydrophobic. Results on these beads are seen in Figure S10 while the sample preparation method is detailed in the supplementary information.

Making Glass Beads Hydrophobic

The glass spheres were first cleaned by treating them with the piranha (3:1 H₂SO₄ and 30% concentrated H₂O₂ mixture) solution. The cleaned glass spheres were rinsed with the distilled water multiple times and were left to dry. The dried clean glass spheres were then poured in a mixture of isooctane and FOTS (fluorooctatrachloro-silane) solution. The top portion of the container was closed with the wax tissue and was put in an ultrasonicator. After 30 minutes of the treatment the glass spheres were taken out of the container and were put on a pre-cleaned glass plate. The glass plate was kept in an oven where the wet glass spheres were heated at 70⁰C for 6 hours. The evaporation of the silane leaves a thin film around the glass spheres making them hydrophobic. The glass beads were turned once to get the hydrophobic layer uniformly around them.

Sample Preparation with Hydrophobic Glass Beads

The porous medium was created by mixing the prepared hydrophobic glass spheres with the DI water. Experiment was conducted in a glass beaker with a diameter of 4 cm. The sample was ~5cm high. Heat received by the porous medium top surface was ~2000 W/m². In this case, water level was always kept higher (than the top most glass beads level) which prevents the hydrophobic spheres from popping up to the water surface. Care was also taken while dropping the hydrophobic spheres in water so that no air was entrained along with them in the liquid. The experiment was stopped when no significant mass loss was observed. Surprisingly, the porous medium was found crusted throughout the height unlike with the hydrophilic ones where the crust was limited to a few layers near the top exposed end.

Treatment of Natural Sand

Apart from the nearly-monodisperse particle sizes, an experiment was also conducted with sieved natural sand, whose particle diameter ranged from 0.30 to 0.50 mm. Before its use, the sieved sand was oven dried at 350⁰C for two days in order to remove the unwanted constituents. Upon heating, it was slowly cooled, to the room temperature, in order to avoid any condensation. The sample height was approximately 8 cm with an overall porosity of ~43%.

Imaging

Three types of microscopes were used for the imaging purposes. Larger glass beads were imaged using low magnification (maximum 10x) 'Lawrence' microscope. Samples with smaller glass beads were viewed using a high resolution Karl-Zeiss microscope; the magnifications used were 100x and 200x. In the third type, we used a scanning electron microscope for further magnification and better contrast. Along with these three standard types of microscopy, we also used digital cameras (Nikon and Canon) for imaging purposes.

Dye Visualization

We used a unique visualization method for tracking the evaporation sites. The benefits of this new type of method, using fluorescein particles as dye, has been explored recently [25-27,46]. The particles are originally orange in colour but turn water green when mixed with it. Conversely, a fluorescein dye mixed water solution will slowly turn orange upon evaporation. Thus, the solid regions, where water has fully evaporated, are left with the deposited fluorescein particles. Interestingly, the regions from where water has been drained (either by gravity or by capillary films) would finally correspond to the original colour of the solid

particles used in preparing the porous medium; in our experiments it is white, the true colour of glass beads.

Results and discussion

Characteristic curves and the time of hardening

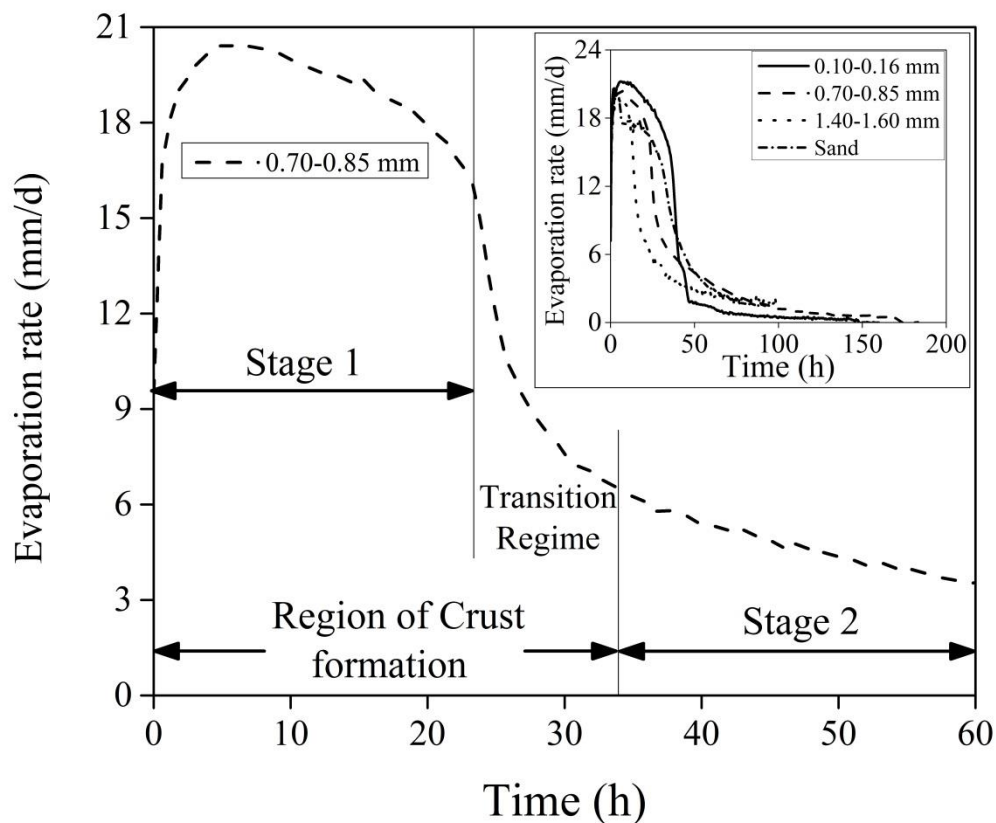


Figure 1 Variation of the evaporation rate versus time for the glass beads with 0.78 mm diameter. Curves for the other cases are seen in the inset. Heat flux received by the top surface in all the cases was $\sim 1000 \text{ W/m}^2$.

We briefly discuss the process of drying from a typical experiment. Figure 1 shows the variation of the rate of evaporation, of water, from an initially fully saturated (when all the voids in the porous medium was occupied by the liquid) porous medium consisting of 0.78 mm diameter glass beads. The heat flux received by the porous medium top surface was $\sim 1000 \text{ W/m}^2$. In the presence of this heat, the evaporation rate increases rapidly and reaches $\sim 20 \text{ mm/day}$ (at ambient relative humidity of $\sim 60\%$) within 3 hours; this value is about the same as that from bare water surfaces and is known as the ‘potential’ evaporation rate. High evaporation rates are sustained in stage 1 (see Figure 1) even as the porous medium dries. The high rates of drying are maintained by the capillary films which maintain the continuity between the water near the exposed end and continuously receding (within the porous medium) drying front. The presence of distinct wet patches were clearly seen using an IR camera [25,26,28] as seen in Figure 2. With time these wet patches shrink (see Figure 2) and eventually vanishes from the exposed surface. At this instant the porous medium enters stage 2 of evaporation. For the glass beads with 0.78 mm diameter, stage 1 is sustained (see Figure 1) till ~ 23 hours. The rate of drying drastically decreases in the transition regime (at the end of stage 1) and eventually takes a much lower value in stage 2. Crust forms during both the

stage 1 of evaporation and in the transition regime. Similar curves of the evaporation rate for a few other porous media are seen in the inset of Figure 1. Apart from the evaporation rate (Figure 1), the other evaporation characteristics curves (temporal variation of mass loss due to evaporation and the near-surface temperature) are seen in Figure S4-S6. A reduction in the evaporation rate is followed by an increase in the surface temperature. In stage 2 of evaporation, the surface temperatures are seen much higher than their values in the stage 1; this depends on the amount of heat intercepted at the porous medium top surface.

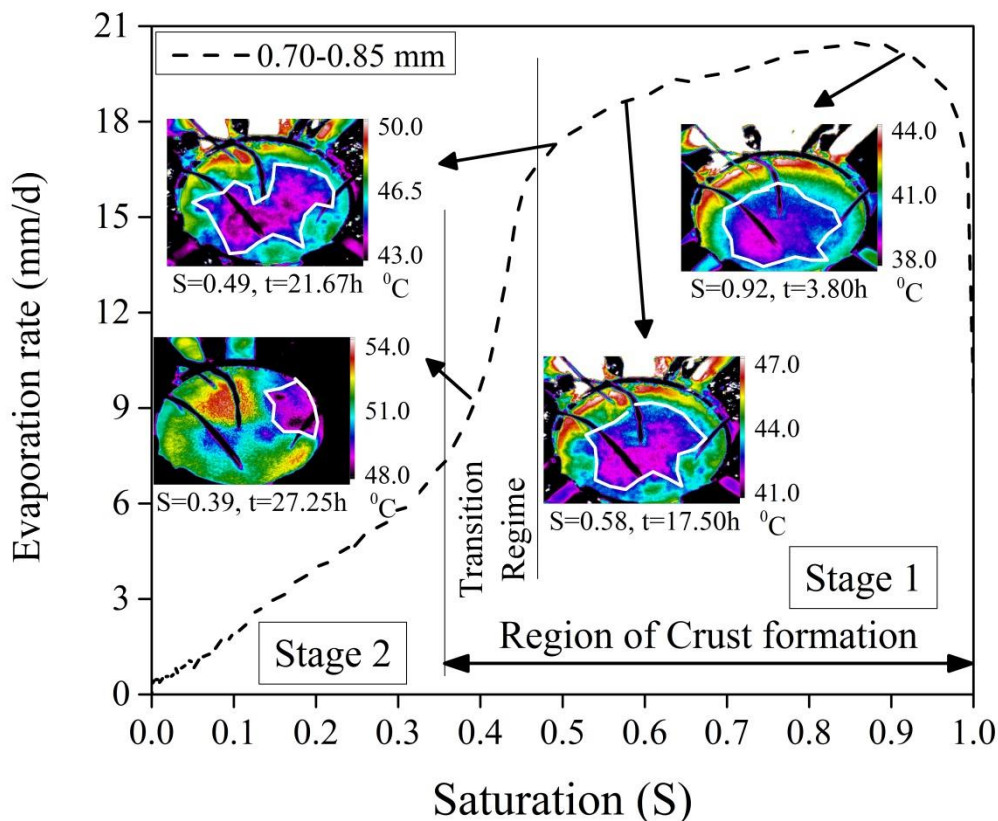


Figure 2 Rate of evaporation versus the saturation (S) for the case of 0.78 mm diameter glass beads. The experiment is same as in Figure 1. IR images corresponding to four important instants are also seen. White curved lines in the IR images represent the boundary between the completely wet (inner) and the completely dry regions on the surface of the porous medium. Also mentioned are the temperature scales for the IR images.

Figure 2 shows the variation of the evaporation rate, from 0.78 mm diameter glass beads, versus the percentage of remaining water or saturation (S). The curve should be seen *from right to left*. At $S=1$, the porous medium is fully saturated; the instant where the experiment began. With time, the porous medium loses water and S decreases. The IR images taken from the above, of the porous medium top surface, are also seen in Figure 2 at four distinct instances. For clarity, these IR images have been marked with the corresponding S values, the experimental duration, and the (dynamic) temperature scale at their right side. White lines in these images separate the ‘wet’ and ‘dry’ regions [25,26,28]. Note that the region within the white line reduces with time (decreasing saturation values) and eventually vanishes at the end of the transition regime (this marks the beginning of stage 2 of evaporation); this has been recently named ‘*shrinking wet patch*’ pattern [25]. In connection with the formation of the hardened surface layer, we observed that the region outside the white line was already crusted (even at S value as high as 0.90) while the region within the white line was soft (even at S as low as 0.40). We conclude that the low temperature region in

the IR images represent the relatively wetter zone which are soft while the higher temperature regions are hard. The definition and determination of either hard or soft layer is discussed next. Note that the crusts (hard layer) starts forming as soon as water started moving from the relatively larger pores to the smaller ones.

Before discussing the results of hardened surface layer in detail, we must tend to, in short, the question *when crusts form and how to determine whether they are hard or not?* Previously, we concluded that the hard layer starts forming as soon as the porous medium begins drying. For the other question, viz., to ascertain how hard is the crust, an experiment was conducted with water and 0.13 mm diameter GB in a small container. A higher density stainless steel (SS) ball, 1 mm in diameter, was dropped, at different instants, from a height of ~10 cm. Initially (when the porous medium was fully saturated) the ball didn't bounce and made an indent (Figure S3) where it landed; this essentially signifies the softness at the beginning of the experiment. After some time, on the relatively drier regions (similar to the regions outside the white line in the IR images in Figure 2), the ball bounced back (Video S1 and S2) indicating the harder top surface; the porous medium was evaporating in stage 1 at this instant. This clearly indicates the crusted layer formed at the top well before the experiment finished; this conclusion is in line with the explanation of Figure 2. Balls bouncing on the crusted top surface are seen in a much better way with multiple balls (Video S3). We now discuss the formation of crusts (based on the direct experimental observations) for the various cases and we also present a simple (visual-based) method to determine the crust's thickness. During the passage we also explain, at the pore scale, where the crusts form and the reason for them.

Drying in the presence of external IR heating

We now present experimental evidences of the crust formed near the evaporating end; these crusts are only a few particle diameters thick. Crusted surfaces were clearly observed in all the cases with the external heating. Crusts were not observed when the samples were not externally heated. Figure 3 shows the condition at different locations of porous media at the end of the experiment. These experiments were carried out in a 6.3 cm diameter glass beaker. The water-saturated sample heights in all the cases were between 8-9 cm and DI water was used as the evaporating liquid. Heat flux received by the porous medium top surface was ~1000 W/m² in all the cases. The average surface temperature in stage 1 (wet patch period [25]) was between 36⁰C and 42⁰C while in the stage 2 (dry surface) it was close to 60⁰C (see Figure S5). The experiment was concluded either when the porous medium stops evaporating or when the evaporation rate reduces to a very low value i.e. 1-2 mm/d.

Figure 3 shows the conditions of the samples at the end of the respective experiments. At this instant, the porous media were dry except for the tiny liquid bridges between the particles where water was trapped in the form of the pendular structures. Figure 3a shows the thin crusted sample, with 0.13 mm diameter glass beads, broken in multiple parts; they broke like a cookie. Initially the entire top surface was hard which was removed carefully. This larger crust (~6 cm diameter and ~2 mm thickness) did not break when held (with fingers on the top and at the back near the periphery) horizontally or vertically. Clusters of spheres were also held by the liquid bridges at deeper regions (away from the top surface) but, unlike the crusts, they are seen as 'clumps' (Figure 3c) similar to the sandcastles. The crusted pieces (Figure 3a) however were much harder than the clumps (Figure 3c). Obviously unlike the crusts, these clumps could not be held between the fingers as they fell apart. Similar to the 0.13 mm diameter GB case, crusts were also found (see Figure 3b) with 0.78 mm diameter glass beads. Interesting point to note here is the sticky nature of the crust with the container wall. After the end of the experiment a few holes were made on the top crusted layer. Apart

from the spheres present in the crust (~ 4 mm thick), the remaining spheres below the crust (~85 mm high) were removed, after tilting the container, through the holes in the crust. The image (Figure 3b) is a result of following this procedure. Note that in both glass bead cases the crust was very thin and in fact was limited to a few numbers of layers at the evaporating end. Surprisingly, with the natural sand the crust was not limited to a few layers but occupied the entire column height. We believe that this unique feature occurs due to two reasons: (a) presence of multiple particle sizes and (b) irregular geometry of the sand particles. These two reasons enhance the contact area between the particles which must have provided additional strength for the crust to span the entire porous column. The more detailed information and discussion regarding the results of the experiment with the natural sand are given in the supplementary information.

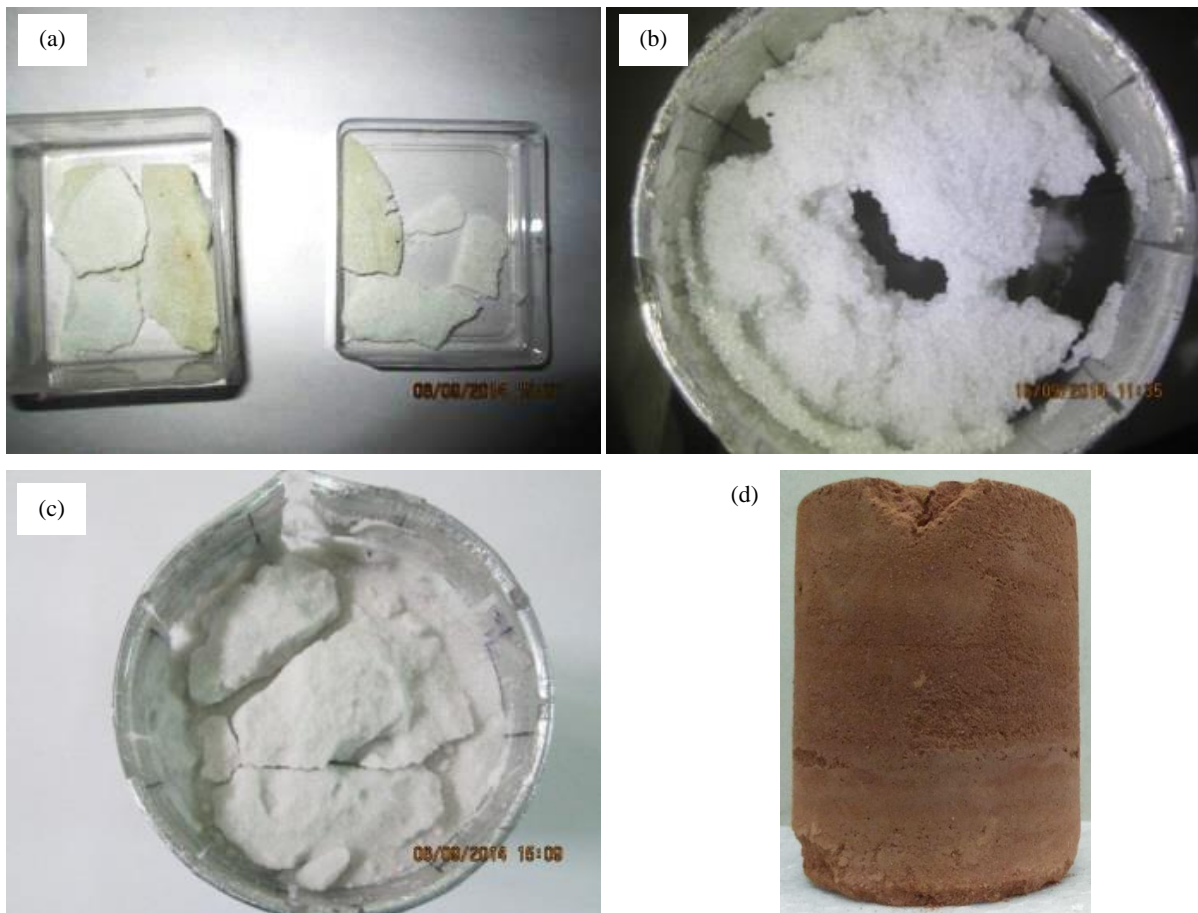


Figure 3 Images at the end of the experiments with different samples. Crusts, formed within a few top layers, in the case of (a) 0.13 mm and (b) 0.78 mm diameter glass spheres respectively. Clumps, similar to sandcastles, rather than the crusts are seen (c) at the deeper locations away from the top exposed surface. Crust in case of the natural sand (d) is not limited to a few layers near the top but covers the entire column height. Heat flux incident on the porous media top surface in all the above experiments was $\sim 1000 \text{ W/m}^2$.

The microscopic images seen in Figure 4 present a better picture of the crust (and its strength). Figure 4a, taken at 200x magnification clearly shows the isolated water (which may also contain some impurities) trapped, acting as a liquid bridge, between two 0.13 mm diameter glass beads; these water bridges are marked '1' and '2' in the image. The water bridge is not seen when the spheres were separated by some distance; this gap is $\sim 10\text{-}15 \mu\text{m}$. This clearly means that during evaporation process, a water bridge can only be trapped if two spheres are in contact at the level of surface roughness. Note that water is also trapped between the beads and the container wall (not shown here). Similar liquid bridges between

spheres in contact are seen (Figure 4b) for the case with 0.78 mm diameter glass beads; this image was taken at 8x magnification. Water bridges were also observed in case of 1.40-1.60 mm diameter glass beads (Figure S7a). The SEM images, taken of the crust with 0.13 mm diameter glass beads, shows clear and detailed picture of the liquid bridges (Figure 4c,d) and the condition of the beads. Some impurities are also seen deposited on the glass beads' surface (and possibly in the water bridges); these impurities may have come either from the sample or from the atmospheric air or both.

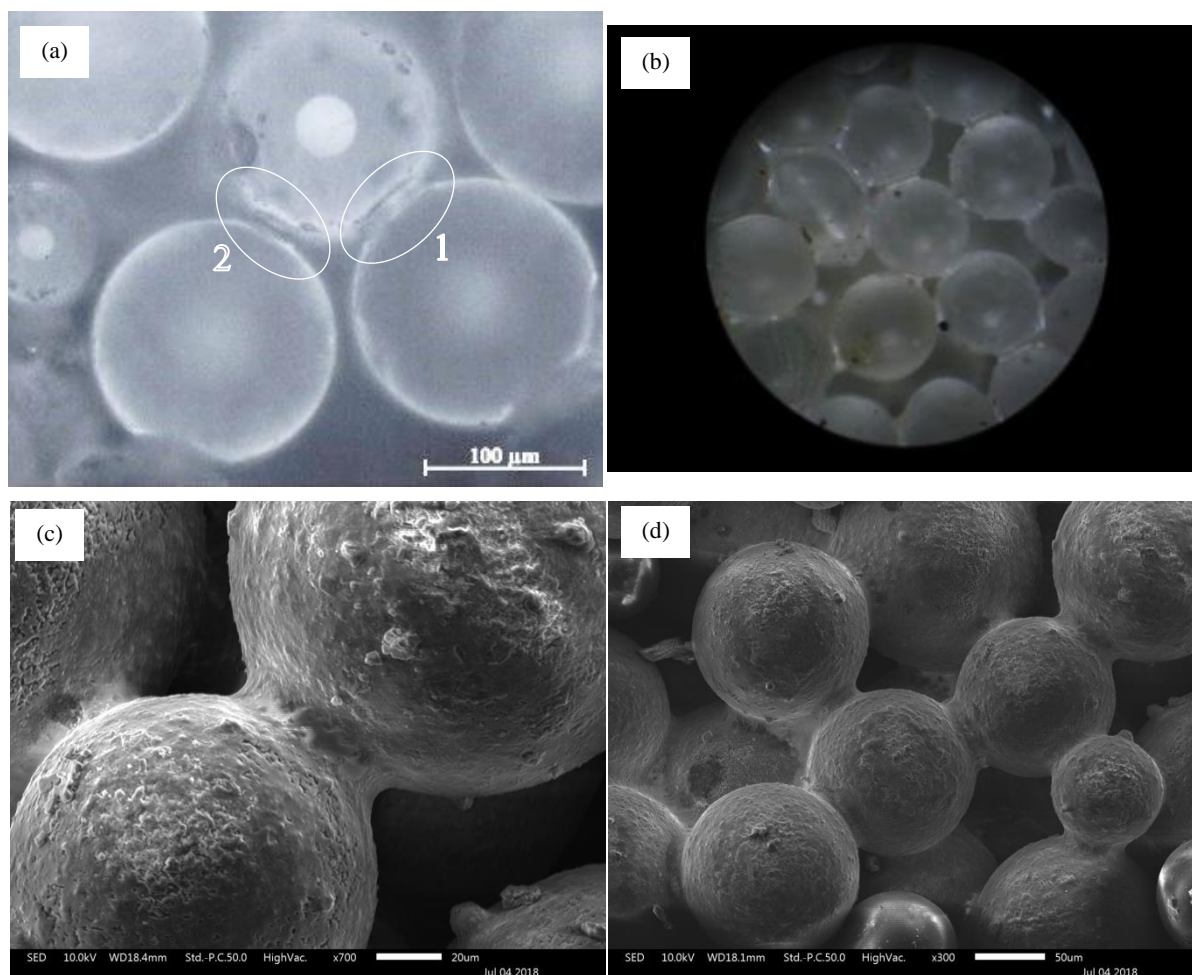


Figure 4 SEM images showing (a) a liquid bridge between two 0.13 mm glass beads and (b) multiple liquid bridges. Microscopic images of the crust (a) are seen in (c) and (d) at 100x and 200x magnifications respectively. Traces of water between the glass beads are clearly seen in these images.

Next we look at the process of the formation of the unevaporated liquid bridge (which was found in the crusted samples discussed earlier). For this we devised a controlled system consisting of a single liquid bridge trapped between two 3.00 mm diameter glass beads in contact. DI water was coloured green using the fluorescein dye for better visual contrast. The beads were constrained which restricted their motion. It is important to understand the evaporation from such a basic system since this is what must be happening, at multiple locations, in the large scale experiments. The microscopic images (Figure S9) shows, with time, the shrinking liquid bridge and (eventually) a thin unevaporated region which did not evaporate even after many days. A video (Video S4) shows the drying of this trapped meniscus up to the unevaporated part. Similar phenomenon is expected to occur in the large scale experiments i.e. the contacts between the beads indeed retain some water which remain unevaporated. The reason for the unevaporated water content needs further investigation. It is clear that the presence of water is one of the major reasons behind the crust formation and its

strength similar to the ones observed in the sandcastles and mud-peels. An important difference between these two (crust in the present study and sandcastles) systems is the route they take towards stability. In sandcastles water is added while in the crusts trapped water is a result of evaporation.

We now discuss the rough estimates of the amount of water trapped in different zones at the end of the experiment. In the experiment with the 0.13 mm diameter glass beads, the crust contained ~1.5% (by weight) of water while the clumps retained only about 0.1% (by weight) of water; a total of ~0.5g of water in this experiment did not evaporate even after seven days of heating (see evaporated mass versus time curve for this experiment in Figure S4). The weight percentages of water left in different zones of a porous medium are discussed in detail in the quantitative analysis section. The weight percentage of trapped water in the crust was measured using a precision weighing scale. For the clumps, its weight percentage was calculated based on the total water trapped, water in the crust, and height of the sample. We report, in brief, observations from a few other intuitive experiments, which are directly related to the strength of the crusts. These are:

- (1) The crust was weaker for the larger bead sizes. With 2.50-3.00 mm diameter glass beads the crust did not even form.
- (2) A separate experiment was conducted where the glass beads and the glass beaker were cleaned using the piranha solution and millipore water was used as the evaporating liquid. Crust (weak) formed in this case was due to the water trapped between the beads; though trapped water was not seen clearly (Figure S8a).
- (3) Crust formed (with external heating) with acetone (Figure S8b) was much weaker compared to that with water. The interfacial surface tension is therefore crucial in determining the crusts' strength.
- (4) We didn't notice any significant evidence for the mudcracks in the experiments with the glass beads. Nearly mono-disperse particle sizes and a relatively lower porosity value ($36.5 \pm 1\%$) in the experiments may have drastically reduced the particle's motion during the evaporation process thereby avoiding the mudcracks.

We have shown, till now, that crusts (hardened layer) are formed during the drying of various porous media heated from above. Unheated samples did not produce any significant crusts. We have also shown that the crusts form due to the unevaporated liquid trapped between the contacts of the spheres. Crusts are harder in case of fluids with higher surface tension. The crust is much stronger if the porous medium consisted of a range of irregularly shaped particle sizes such as sand and soil.

Water content in the crust

We have established, using the microscopic, SEM images, and mass of the measured crusted samples, the fact that the crusts' strength is due to the water trapped between the particles. Henceforth an attempt was made to precisely quantify the trapped water content qualitatively and quantitatively.

a Qualitative analysis

In order to further strengthen the claims, a qualitative approach was taken. Fourier Transform Infrared Spectroscopy (FTIR), a standard technique, which is used to determine the types of bonds in any samples, was used to obtain the absorbed infrared spectrum of the crusted sample; obtained with heating the porous medium. The wavenumber range spanned by FTIR was from 4000cm^{-1} to 400cm^{-1} and the corresponding wavelength is between $2.5\mu\text{m}$ to $25\mu\text{m}$.

The Transmittance of the crusted sample is plotted against the wavenumber as seen in Figure S12a. Generally a FTIR spectrum is divided in two halves around 2000cm^{-1} ; our interest lies in peaks at wavenumber larger than 2000cm^{-1} . Four distinct transmittance peaks are seen corresponding to wavenumbers of 2360, 2831, 2943, and 3315cm^{-1} respectively. These peaks were also found with other crust samples consistently. The peak corresponding to 2360cm^{-1} , a weak peak, represents the presence of asymmetrical stretched CO_2 bond. Peaks of 2831 and 2943cm^{-1} correspond to the presence of stretched $-\text{C}-\text{H}$ bond in the crusted sample. Of more importance is the strong peak at 3315cm^{-1} which clearly indicates the presence of water in the crusted sample. In FTIR spectrum a strong peak close to 3300cm^{-1} [48] also represent a few other functional groups such as stretched $\equiv\text{C}-\text{H}$, $-\text{OH}$ in alcohols and carboxylic acids, the existence of whose is impossible in the present experiments. FTIR spectrum was also produced (Figure S12b) for a dry sample. Obviously, the peak representing water corresponding to 3300cm^{-1} wavenumber is missing in this case.

b Quantitative analysis

Curiosity arises regarding the amount (or volume) of water trapped in the crusted samples. We put the crusted samples in an oven at 250°C for 1 day. No physical change in the crust was observed and the particles were still sticking to one another. We performed thermogravimetric analysis (TGA) of the crusted samples where both the mass loss and the chamber temperature were simultaneously monitored. Note that the crusted samples, Figure 3a, were initially crushed to get a small (nearly 20 mg) piece and was quickly placed inside the instrument.

The atmosphere in the sample chamber was purged with nitrogen to avoid oxidation or other undesired reactions. Once the weighing balance stabilized, the temperature of the chamber was increased at a rate of $5^\circ\text{C}/\text{minute}$. The maximum temperature of the sample chamber was set to 540°C in order to avoid any physical change in the glass spheres. The mass and temperature data were recorded every 0.1 seconds. One of the experiments was conducted with unused (dry) 0.13 mm diameter glass spheres to check for the accuracy of the measurements in case of a dead weight. These experiments were repeated to get the consistent trends.

Figure S13 shows the variation of the percentage mass loss, ' m_p ' (primary vertical axis) versus the chamber temperature for the crusted sample. Note that the maximum average surface temperature in evaporation experiments was about 60°C (see Figure S5). Cooling-led condensation increases the trapped water content in the crusted sample. This extra condensed water evaporated rather easily. A peak in the mass rate curve (secondary vertical axis) for the crusted sample is seen at $\sim 70^\circ\text{C}$. Note that such a strong peak was not seen (data not included here) in case of the dry sample. Mass loss at temperatures higher than 100°C is observed possibly due to enhanced potential energy of trapped water thanks to the sharp menisci. The other mass rate peak, corresponding to 310°C , is due to the evaporation of adsorbed water; this peak was seen in both the samples. Nearly 1% of the mass loss is seen occurring till 100°C majority of which would have been the condensate water. Out of the total mass loss of 2.5% we can thus say that 1.5% of water was trapped originally in the crusted sample when the sample was not cooled; samples would automatically cool down once the IR heater is switched off. It is interesting that such tiny water content leads to enormous increase in the overall strength of the crusts. We now investigate a key property of the crusts viz. crust thickness, for which we propose a unique strategy for this purpose in the next section.

A unique method to determine crust thickness

Water is trapped between the spheres either when water is leaving (preferential motion of water) a particular region or is evaporating. These regions can be distinguished, as in Figure S9, [25] if a coloured solution is used. A small (larger than a two-sphere-system and smaller than the large scale system) scale experiment was designed to see the colour patterns in an evaporating porous medium. This experiment was performed with 0.13 mm diameter glass beads and coloured (using orange colour fluorescein dye) water in a small Teflon box. Diameter of the Teflon box was ~4 cm and the height of the sample was ~1.5 cm. Initially the porous medium appears green throughout (Figure 5a) due to the presence of the fluorescein particles in the solution phase. Capillary film(s) brings water, and fluorescein dye, from deeper regions of the porous medium to its top where water evaporates leaving the fluorescein dye deposited on the beads surfaces. Since fluorescein dye particles are orange, the distributed deposited dye appears orange (Figure 5b). The crust formed in this experiment was broken and seen (Figure 5b) as a thin layer, 1-2 mm (10-20 layers), consisting of nearly all the fluorescein dye used in the experiment. Crust bottom, inverted pieces in Figure 5b, and non-crust regions (below the crust) both appear white, the true colour of the glass beads.

Factors affecting the crust thickness

Deposited fluorescein dye in Figure 5b also shows that during stage 1 almost all the evaporation must occur within a thin layer near the exposed end of the porous medium. Since the particles would keep depositing (owing to drying) within these layers it is obvious that these layers form the crust. We now investigate the dependence of the crust thickness on various controlled parameters such as the particle size and the incident heat load (linked to the porous medium surface temperature). For studying the effect of varying heat flux, one set of experiments were conducted in small Teflon boxes, having a removable bottom, consisting of 0.13 mm diameter GB as seen in Figure 6a. Difference in sample's distance to the IR heater ensured different incident heat fluxes (this is governed by the varying view factors for different samples). Figure 6b shows the porous media top surfaces (of the four samples) after the experiment. The uncrusted particles, seen in Figure 6c were easily removed after the experiment leaving only the crusted layer attached to the container wall (Video S5). This was required since the crusts in the previous experiments were needed to be broken (Figure 3a, Figure 5b) for their removal.

Table 1 shows a list of different types of experiments performed for this study. The saturated and unsaturated bulk densities of the samples across all the experiments varied within a small range 1.51 ± 0.08 and 1.20 ± 0.10 g/cc respectively. The average porosity of the samples was 36.5% with a narrow variation of $\pm 1.5\%$. Crust thickness was calculated based on two different methods: (1) mass measurement of the crust and (2) fluorescein dye deposits. The average crust thickness [cm] was estimated, following a series of steps. These are,

$$\text{Average sample height [cm]} = \frac{\text{Total saturated mass of the sample [g]}}{\text{Saturated bulk density [g/cm}^3\text{]} * \text{Cross sectional area [cm}^2\text{]}} \quad (2)$$

Here, the total saturated mass of the sample [g] is the addition of the masses of the glass beads [g] and the saturated mass of water [g].

$$\text{Saturated bulk density [g/cm}^3\text{]} = \frac{\text{Glass beads mass [g]}}{\text{Saturated water mass [g]} + (\text{Glass beads mass [g]}/2.5)} \quad (3)$$

The value 2.5 in Eq. (3) represents the density [g/cm³] of a single glass bead.

$$\text{Average crust thickness [cm]} = \frac{\text{Crust mass [g]}}{\text{Crust density [g/cm}^3\text{]} * \text{Cross sectional area [cm}^2\text{]}} \quad (4)$$

Next we estimate the unsaturated bulk density i.e. density of the cluster of glass beads in the absence of water.

$$\text{Unsaturated bulk density [g/cm}^3\text{]} = \frac{\text{Glass beads mass [g]}}{\text{Average sample height [cm]} * \text{Cross sectional area [cm}^2\text{]}} \quad (5)$$

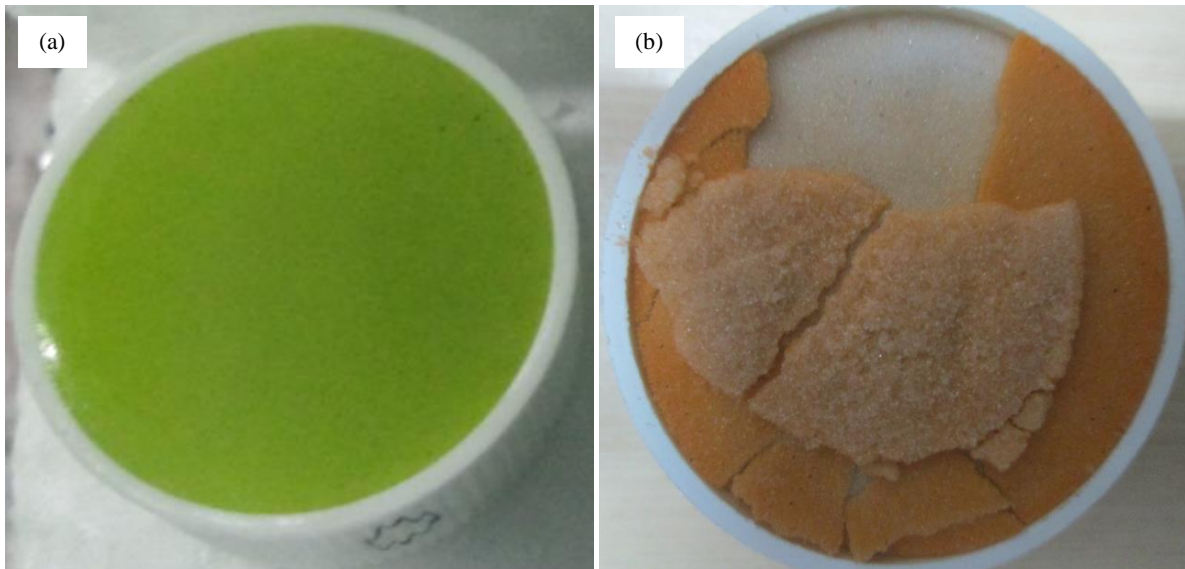


Figure 5 Experiment with fluorescein dye and 0.13 mm diameter glass beads in a small Teflon container is green throughout initially (a). The crusted thin upper layer is clearly seen in (b) at the end of the experiment. The lower regions of the porous medium do not show any significant deposition.

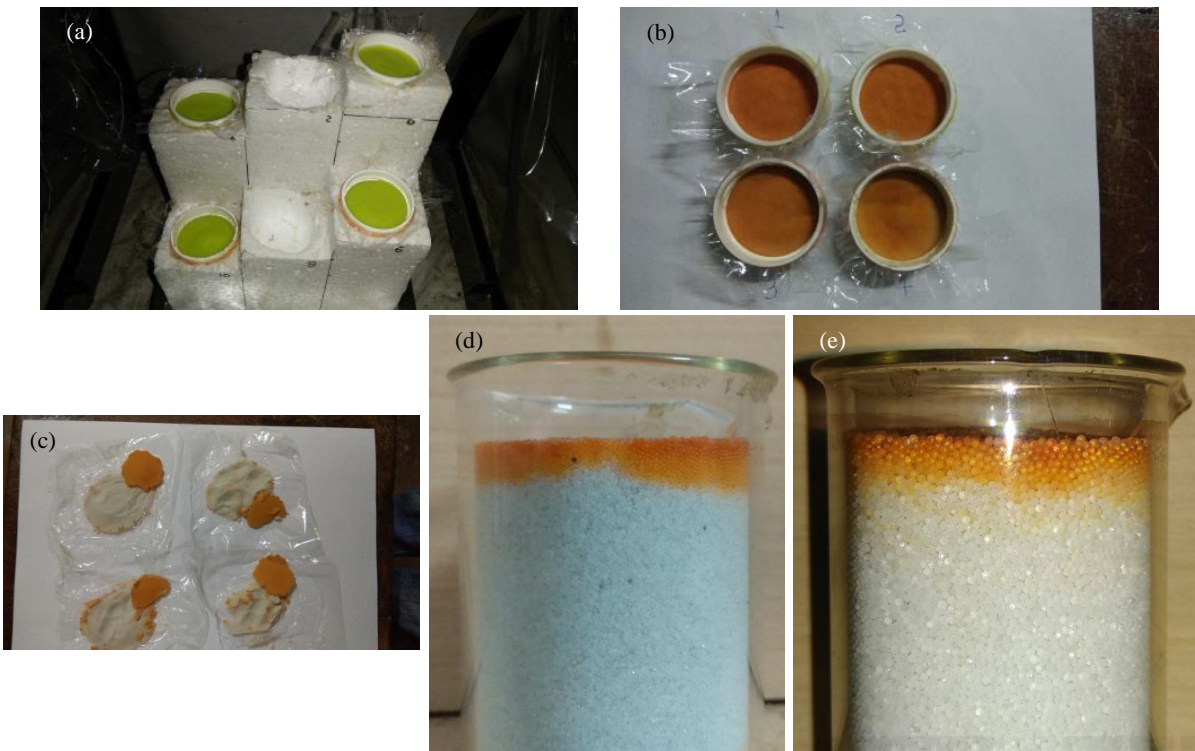


Figure 6 Snapshots showing the condition of samples of crusts for different incident heat fluxes. Different glass bead sizes were used for this study as well.

Sample no.	Glass beads diameter (mm)	Incident heat flux (W/m ²)	Column Height (mm)	Avg. surf. temp. in stage 1 (°C)	Crust / deposited dye thickness (mm)	No. of layers
1	0.13	1400	9.7	44.5	1.8	17
2	0.13	1200	9.9	42.5	2.3	21
3	0.13	1000	9.9	40.0	2.5	24
4	0.13	700	9.7	36.0	2.2	21
5	0.13	500	9.7	32.5	2.9	25
6	0.13	0	9.7	25.5	8.8	84
7	0.13	0	62.9	25.5	12.6	120
8	0.45	1400	9.4	44.5	3.8	9
9	0.45	1200	18.5	42.5	4.7	11
10	0.45	0	64.3	25.5	32.2	69
11	0.78	2000	87.2	50.5	7.6	16
12	0.78	1000	87.3	40.0	10.7	21
13	0.78	500	86.8	32.5	17.5	29
14	0.78	250	84.9	29.5	26.3	38
15	0.78	0	53.6	25.5	37.8	51

Table 1 Experimental parameters of the present study. Experiment with sample numbers '1-6' and '8' were conducted in small Teflon boxes, '9' in a medium size acrylic container, and '7' and '10-15' in larger glass beakers. Hard layer thickness for the corresponding experiments is also mentioned. Average surface temperatures in stage 1 of evaporation are mentioned as a guide.

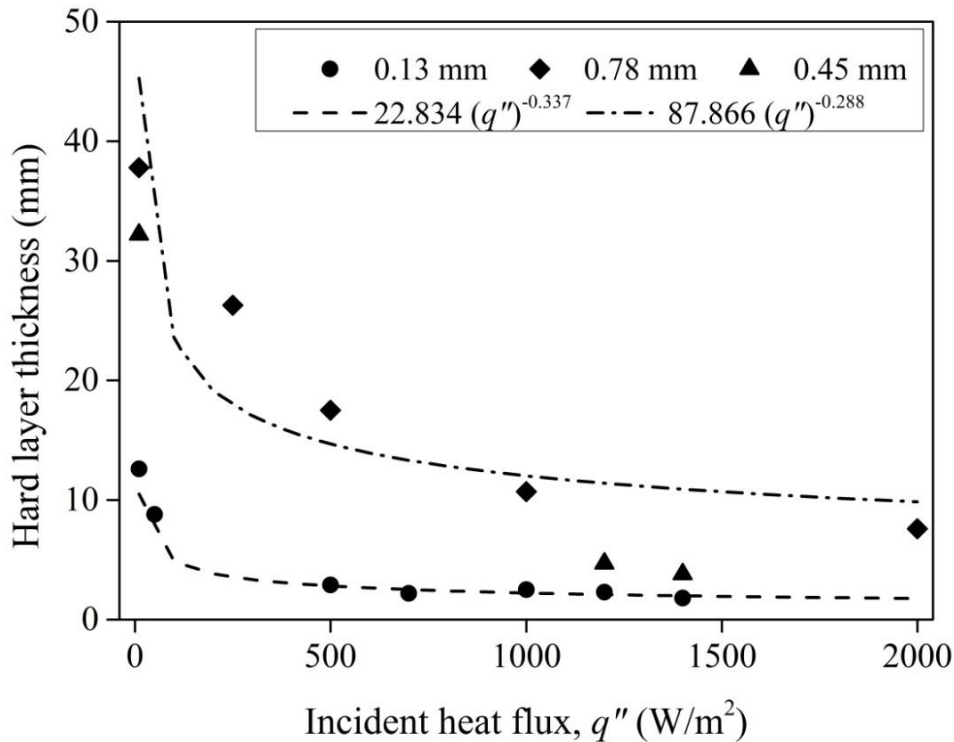


Figure 7 Variation of the thickness of the near-surface hard layer formed in different experiments as a function of the particle sizes and the incident heat fluxes.

The estimated unsaturated bulk density is assumed to be the same as the crust density, which is valid for a large number of particles and layers in the crust. However even for smaller number of layers the deviation from the true value (from larger number of layers) is small (2%). Note that while estimating the unsaturated bulk density, small traces of trapped

water and fluorescein dye in the crust was ignored since their contribution is negligible. The experimental parameters for the current study used to estimate the crust thickness and number of layers in it are seen in Table 1. A few experiments (sample numbers '8' and '9') were conducted with 0.45 mm diameter glass beads in different containers. Experiments with sample numbers '6, 7, 10, and 15' were conducted without external heating. Small container experiments were not performed for 0.78 mm diameter glass beads.

Average crust thickness was nearly 2 mm in (the majority of the) experiments with external heating in small Teflon boxes (see Table 1); irrespective of particle size and heat flux; the difference in crust thicknesses across the experiments is minute. Crust was very weak in experiments without the external heating and could not be removed cleanly. For these experiments deposited fluorescein dye layer thickness hold more meaning. Crust thicknesses for these non-heating cases are much higher than their heating counterparts. In the non-heating case the deposited dye thickness is seen increasing with the increasing glass bead size. With external heating nearly same deposited thicknesses (~ 5 mm), see Figure 6d-e, were observed for 0.45 mm and 0.78 mm diameter glass beads; these experiments are not mentioned in Table 1. Figure 7 shows the relation between the incident heat flux (q'') and the obtained hard layer for different particle sizes. Two major conclusions can be drawn (a) the crust thickness increases at lower q'' and (b) larger beads give thicker crust for a fixed q'' . The experimental data is fit using a power law as seen in Figure 7. The exponent of crust thickness (in 'mm') and q'' (in 'W/m²') curve is about -0.30 for all the three glass bead sizes investigated. Interestingly, evaporation rate in stage 1 of evaporation was found to vary nearly linearly with q'' (*unpublished*) which can be obtained using a simple surface energy budget [25,26,46]; discussing this relation here is not in the interest of present study. In a completely different system, where mud-peels' thickness was theoretically obtained [45], the exponent of mud-peel thickness and the evaporation rate was -0.67. Note that for those experiments where no external heating was done, we calculated q'' directly from (hotter) ambient temperature and the wet bulb temperature.

Conclusions

Similar to caking, we report the formation of crust (hard layer) during evaporation from different types of porous media. Unlike sandcastles, the crusts with glass beads were found not to deform when applied a load rather they broke much like a piece of cookie. Strength-wise these crusts can be treated similar to mud-peels except in the present study they formed even in cases where 'leaching' was avoided. The present investigation thus focussed on the reasons, apart from leaching, behind the crust formation. The formation of the crust can be due to any of the following factors: (1) surface tension, (2) electrostatic force, (3) mechanical locking, (4) van der Waals forces, and (5) hydrogen bonding. Of course, any combinations of these five factors would further strengthen the crust. However, the magnitudes of the van der Waals, electrostatic, and hydrogen bonding forces are several orders of magnitude smaller than the interfacial surface tension force. Factors, such as the effects of particle size, heat flux, particle size variation, and the hydrophobicity of the porous medium (see methods section in Supplementary information), influencing the crust strength and its thickness were also investigated.

Weak crust (in glass beads) with acetone compared to water indicates that along with the hydrogen bonding between beads surface and water, the magnitude of the surface tension too played a major role in strengthening the crust. Mechanical locking (which is very important in case of randomly shaped range of particles in sand) and van der Waals force seems unlikely to contribute towards the overall strength. Results from the experiment with clean glass beads in a clean glass beaker using millipore water as the evaporating liquid showed that the impurities, though cannot be completely ignored, did not play a major role

thereby eliminating the existence of the electrostatic force. Dominant contributor is surface tension between the trapped water content and the beads surface. Microscopic and SEM images (showing remarkably detailed view of the liquid bridge) clearly showed the presence of water trapped in the contacts of the beads. Presence of water in crusted samples was also confirmed using FTIR and TGA.

The strength of the crust in non-heating cases was found to be much weaker than with the heating cases. A possible explanation could be due to the condensation in heating cases which enhances trapped water content while cooling. Crust strength was found to decrease drastically with increasing particle sizes. For particle sizes larger than 1.5mm crust either was very weak or did not exist even though liquid bridges did exist. We found the crust to be limited to a few layers near the top of the porous medium consisting of glass beads and a confirmation was provided by deposited fluorescein dye layer thickness. The exponent of the crust thickness and the incident heat load (or the evaporation rate in stage 1) was obtained to be about -0.30; we do not have a theoretical basis for this behaviour. However, in case of natural sand experiment, full column was found crusted and its strength was incredibly high. We expect all the factors to contribute considerably in making the crust tougher in this case. Shrinkage leading to detachment of sand particles from container wall was observed in this case unlike the glass beads case where particles were in contact with the container walls and liquid was trapped between them. This unique feature indicates towards the inefficiency during manual packing while preparing a porous medium and it seems as if evaporation or surface tension leads to a lower porosity and thus a better packed structure. A major missing point in the current investigation is the determination of crust strength using some standard techniques. Due to the unavailability of such a method the crusts could not be tested for their strength and the information in the text was completely a hands-on experience, while breaking the crusts. Attempts will be made, in future, to analyze the crust strength in a quantitative way.

Conflicts of Interest

There are no conflicts of interest to declare.

Supporting information

Data, along with the associated videos, required for reproducing the results of this study are available at https://figshare.com/articles/Data_-_Crust_related_experiments/7430897.

Acknowledgements

We thank Robert Centre for Cyber-Physical Systems for funding this research under the grant RBCCPS/ME/JHA/PC-0013. We thank Prof. K.R.Y. Simha (Mechanical Engineering) and Prof. T.N. Guru Row (SSCU) of IISc for their valuable suggestions. We also thank Chemical engineering and Organic chemistry departments (of IISc) for utilizing their experimental facilities. We are thankful to Mr Gautam Revankar who took the SEM images.

Notes and references

1. E. M. Kindle, *The journal of Geology*, 1917, **25(2)**, 135-144.
2. A. Groisman and E. Kaplan, *EPL (Europhysics Letters)*. 1994, **25(6)**, 415.
3. G. Müller, *Journal of Geophysical Research: Solid Earth*. 1998, **103(B7)**, 15239-15253.
4. Z. C. Xia and J. W. Hutchinson, *Journal of the Mechanics and Physics of Solids*. 2000, **48(6-7)**, 1107-1131.
5. L. Pauchard, M. Adda-Bedia, C. Allain and Y. Couder, *Physical Review E*. 2003, **67(2)**, 027103.
6. A. Ghatak, L. Mahadevan, J. Y. Chung, M. K. Chaudhury and V. Shenoy, *In Proceedings of the Royal Society of London A: Mathematical, Physical and Engineering Sciences*. 2004, **460(2049)**, 2725-2735.
7. O. Fenyvesi, *In Conference of Junior Researchers in Civil Engineering, Budapest, Hungary*. 2012, 51-57.

8. E. R. Dufresne, E. I. Corwin, N. A. Greenblatt, J. Ashmore, D. Y. Wang, A. D. Dinsmore, J. X. Cheng, X. S. Xie, J. W. Hutchinson and D. A. Weitz, *Physical Review Letters*. 2003, **91(22)**, 224501.
9. V. Slowik, M. Schmidt and R. Fritzsche, *Cement and Concrete composites*. 2008, **30(7)**, 557-565.
10. V. Slowik, T. Hübner, M. Schmidt and B. Villmann, *Cement and Concrete composites*. 2009, **31(7)**, 461-469.
11. A. F. Routh and W. B. Russel, *Langmuir*. 1999, **15(22)**, 7762-7773.
12. M. S. Tirumkudulu and W. B. Russel, *Langmuir*. 2004, **20(7)**, 2947-2961.
13. M. S. Tirumkudulu and W. B. Russel, *Langmuir*. 2005, **21(11)**, 4938-4948.
14. K. B. Singh and M. S. Tirumkudulu, *Physical review letters*. 2007, **98(21)**, 218302.
15. K. I. Dragnevski, A. F. Routh, M. W. Murray and A. M. Donald, *Langmuir*. 2010, **26(11)**, 7747-7751.
16. W. B. Russel, *AIChE journal*. 2011, **57(6)**, 1378-1385.
17. E. Paquette, P. Poulin and G. Drettakis, *In Proceedings of Graphics Interface*. 2002, **p.10**.
18. C. J. Brinker and G. W. Scherer., *Academic press*, 2013.
19. L. A. Brown, C. F. Zukoski and L. R. White, *AIChE journal*. 2002, **48(3)**, 492-502.
20. M. Bergstad, D. Or, P. J. Withers and N. Shokri, *Water Resources Research*. 2017, **53(2)**, 1702-1712.
21. S. M. Shokri-Kuehni, M. N. Rad, C. Webb and N. Shokri, *Advances in water resources*. 2017, **105**, 154-161.
22. S. M. Shokri-Kuehni, T. Vetter, C. Webb and N. Shokri, *Geophysical Research Letters*. 2017.
23. N. Mitarai and F. Nori, *Advances in Physics*. **55(1-2)**, 1-45, (2006).
24. P. Lehmann, S. Assouline and D. Or, *Physical Review E*. 2008, **77(5)**, 056309.
25. N. Kumar and J. H. Arakeri, *Transport in Porous Media*. 2018, 125(2), 311-340.
26. N. Kumar and J. H. Arakeri, *Water Resources Research*. 2018, 54(10), 7670-7687.
27. N. Kumar and J. H. Arakeri, *Int. J. Thermal Sciences*. 2018, 133, 299-306.
28. N. Kumar and J. H. Arakeri, *Journal of Hydrology*. 2019, 569, 795-808.
29. N. Kumar and J. H. Arakeri, *Int. J. Multiphase Flow*. 2018, 109, 114-122.
30. A. G. Yiotis, D. Salin, E. S. Tajar and Y. C. Yortsos, *Physical Review E*. 2012, **85(4)**, 046308.
31. M. Sadeghi, M. Tuller, M. R. Gohardoust and S. B. Jones, *Journal of Hydrology*. 2015, 1277-1281.
32. D. Or, P. Lehmann, E. Shahraeeni and N. Shokri, *Vadose Zone Journal*. 2013, **12(4)**.
33. C. M. Cejas, J. C. Castaing, L. Hough, C. Fréty and R. Dreyfus, *Physical Review E*. 2017, **96(6)**, 062908.
34. J. Thiery, S. Rodts, D. A. Weitz and P. Coussot, *Physical Review Fluids*. 2017, **2(7)**, 074201.
35. G. Mason and W. C. Clark, *Chemical Engineering Science*. 1965, **20(10)**, 859-866.
36. K. Hotta, K. Takeda and K. Iinoya, *Powder Technology*. 1974, **10(4-5)**, 231-242.
37. D. J. Hornbaker, R. Albert, I. Albert, A. L. Barabási and P. Schiffer, *Nature*. 1997, **387(6635)**.
38. A. Samadani and A. Kudrolli, *Physical Review Letters*. **85(24)**, 2000, 5102.
39. S. Herminghaus, *Advances in Physics*. 2005, **54(3)**, 221-261, (2005).
40. M. M. Kohonen, D. Geromichalos, M. Scheel, C. Schier and S. Herminghaus, *Physica A: Statistical Mechanics and its Applications*. 2004, **339(1-2)**, 7-15.
41. Z. Fournier, D. Geromichalos, S. Herminghaus, M. M. Kohonen, F. Mugele, M. Scheel, M. Schulz, B. Schulz, C. Schier, R. Seemann and A. Skudelný, *Journal of Physics: Condensed Matter*. 2005, **17(9)**, S477.
42. M. Scheel, R. Seemann, M. Brinkmann, M. Di Michiel, A. Sheppard, B. Breidenbach and S. Herminghaus, *Nature Materials*. 2008, 7(3), 189.
43. A. Kudrolli, *Nature materials*. 2008, 7(3).
44. R. W. Style and S. S. Peppin, *In Proceedings of the Royal Society of London A: Mathematical, Physical and Engineering Sciences*. 2010, **p. rspa20100039**.
45. R. W. Style, S. S. Peppin and A. C. Cocks, *Journal of Geophysical Research: Earth Surface*. 2011, **116(F1)**.
46. N. Kumar, *PhD Thesis*, Indian Institute of Science, 2017.
47. M. S. Bobji, S. V. Kumar, A. Asthana and R. N. Govardhan, *Langmuir* 2009, **25(20)**, 12120-12126.
48. D. M. Wieliczka, S. Weng and M. R. Querry, *Applied optics* 1989, **28.9**: 1714-1719.